Comput Mech (2016) 57:701–716
DOI 10.1007/s00466-015-1256-9

ORIGINAL PAPER

A Galerkin-based formulation of the probability density evolution method for general stochastic finite element systems

Vissarion Papadopoulos[1] · **Ioannis Kalogeris**[1]

Received: 24 June 2015 / Accepted: 23 December 2015 / Published online: 9 January 2016

Abstract The present paper proposes a Galerkin finite element projection scheme for the solution of the partial differential equations (pde's) involved in the probability density evolution method, for the linear and nonlinear static analysis of stochastic systems. According to the principle of preservation of probability, the probability density evolution of a stochastic system is expressed by its corresponding Fokker–Planck (FP) stochastic partial differential equation. Direct integration of the FP equation is feasible only for simple systems with a small number of degrees of freedom, due to analytical and/or numerical intractability. However, rewriting the FP equation conditioned to the random event description, a generalized density evolution equation (GDEE) can be obtained, which can be reduced to a one dimensional pde. Two Galerkin finite element method schemes are proposed for the numerical solution of the resulting pde's, namely a time-marching discontinuous Galerkin scheme and the StreamlineUpwind/Petrov Galerkin (SUPG) scheme. In addition, a reformulation of the classical GDEE is proposed, which implements the principle of probability preservation in space instead of time, making this approach suitable for the stochastic analysis of finite element systems. The advantages of the FE Galerkin methods and in particular the SUPG over finite difference schemes, like the modified Lax–Wendroff, which is the most frequently used method for the solution of the GDEE, are illustrated with numerical examples and explored further.

✉ Ioannis Kalogeris
yianniskalogeris@gmail.com

Vissarion Papadopoulos
vpapado@central.ntua.gr

[1] Institute of Structural Analysis and Seismic Research, National Technical University of Athens, Iroon Polytechniou 9, Zografou Campus, 157 80 Athens, Greece

Keywords Probability density evolution method · Stochastic systems · StreamlineUpwind/Petrov Galerkin · Discontinuous Galerkin finite element method · Stochastic finite element analysis

1 Introduction

The first step to studying the evolution of a mechanical system is to make accurate mathematical idealizations of its properties. That is, the parameters of the system (system geometry, materials, etc.), the response parameters (displacement, stress, strain, etc.) and the constitutive laws that couple them, have to be mathematically expressed in such a way that the mathematical model is in good agreement with the physical model. In the past, extensive research has been carried out, in order to improve the structural models and the constitutive laws that govern them, and even though this research lead to improvement in the results, complete agreement with the results from experiments could not be achieved [27,34]. The reason for this lies in the nature of the variables involved in the system. Considering them to be of deterministic nature was a simplification, dictated mainly by the limitations of computational capacity. In order to achieve a more reliable representation of the physical system, randomness in the excitation as well as in the system parameters, such as the material properties, the geometrical parameters and the boundary conditions, uncertainties in their estimation and their spatial variability had also to be taken into account. This became feasible with the progress of computational technology and the corresponding increase of computer power.

In the effort to incorporate randomness in the modeling of structures, the so called stochastic finite element method (SFEM) was developed, which is an extension of the classical

deterministic FE approach to the stochastic framework. Different methods have been developed for treating the response variability calculation in the framework of SFEM, the most eminent of them being the Monte Carlo simulation [37], variants of the direct MCS, such as importance sampling [36], subset simulation [1] and line sampling [21], the random perturbation technique [18], path integral techniques [19,20] and the spectral stochastic finite element method (SSFEM) [14]. Non-intrusive Monte Carlo simulation serves as a versatile stochastic analysis method, which can be employed in any type of problem, with the drawback though, that in order to achieve high levels of accuracy, great computational cost is required. In order to alleviate this often intractable computational burden, customized solution strategies have been proposed for the repeated solution of near-by systems of algebraic equations required in MCS [28,29,38]. Random perturbation technique on the other hand is more efficient but is still unsuitable for problems with strong nonlinearities and/or large parametric variations. Besides that, path integral techniques, despite their analytical power, are so far mostly applied to single degree of freedom systems, whereas numerical difficulties arise when dealing with multi degree of freedom systems. Moreover, intrusive approaches such as the SSFEM has received great attention in the last decade leading to elegant Galerkin-based formulations. SSFEM requires the solution of an augmented algebraic system of equations with respect to the corresponding deterministic one, which can become quite challenging due to the increased memory and computational resources required. This increase in the dimensions of the coefficient matrix to be inverted can be dramatic in certain cases, such as those involving large variations and/or non-Gaussian fields and may lead to a disproportionate increase of the computational cost, especially in real world problems with a large number of dof's. This implication renders in certain cases the SSFEM intrusive solution a more expensive method, compared to non-intrusive brute force Monte Carlo simulation. In a recent publication [38] the numerical performance of intrusive versus non-intrusive methods is critically assessed on the basis of up-to-date solvers and solution strategies, specifically tailored to the needs of these analyses.

As an alternative to the above methodologies, a new method has been recently proposed by Li and Chen [24], namely the probability density evolution method (PDEM), which has been successfully employed in both static and dynamic, linear and nonlinear, stochastic problems. This method is based on the principle of preservation of probability and, in a sense, introduces a new framework in solving the stochastic conservation equation that governs the flow of probability in the system under consideration. Similar type of equations have been studied by Cho et al., Venturi et al. and Wang et al. in computational fluid dynamics with uncertain parameters [39–41] as well as stochastic oscillators [7]. The applicability, however, of these approaches to general structural stochastic finite element systems has not yet been addressed. The distinction between these approaches and PDEM is that in PDEM the stochastic differential equation is re-derived from the random event perspective [4]. This way a generalized density evolution equation is defined (GDEE), which is further reduced to a one-dimensional pde, which is numerically tractable. A great advantage of PDEM is that it can achieve high levels of accuracy, independently of the problem under consideration and the random parameters involved in it, with the requirement of a relatively small number of repeated deterministic analyses compared to Monte Carlo Simulation.

A key aspect of PDEM lies in solving accurately the resulting deterministic pde's. These pde's express mathematically the conservation of probability and have the form of pure advection, that is, there is no diffusion term in the equations. In such cases numerical finite difference solutions tend to be unstable, unless some diffusion is added artificially in the scheme. Upwind methods, introduce such artificial diffusion, but, even though they lead to a numerically stable formulation, they may result in a considerable "smearing" of the solution [12,22,31,33]. Moreover, in many practical applications the initial conditions involve discontinuities (shock, sharp jumps) and resolving these discontinuities may produce 'unwanted' wiggles (spurious oscillations). In [24] a modified version of the Lax–Wendroff (LW) finite difference scheme, enhanced with the Total Variation Diminishing (TVD) property, is proposed for solving the pde's. This scheme is proven very efficient and numerically stable, but can be prone to overly diffuse solutions. Besides that, in order to ensure its stability, the well known Courant–Friedrichs–Lewy (CFL) [11] condition is necessary to be satisfied. This condition defines the incremental step of the scheme, with the subsequent increase in the computational cost.

In an attempt to improve the accuracy of the LW finite difference schemes, an alternative numerical solution of the PDEM is proposed in this paper, which is based on a Galerkin finite element method approximation. More specifically, we formulate the GDEE in the framework of time-marching DG scheme [8–10,15,32], as well as SUPG FE scheme [2,13] for the solution of the corresponding pde's. Numerical results are presented, which demonstrate that the use of the SUPG, endowed with a shock capturing term [17], provides more accurate results with respect to LW and DG, especially in the areas near the boundary conditions at practically lower computational effort. The decrease in the computational effort is mainly attributed to the fact that the SUPG method is not restricted by the CFL condition. In addition, a reformulation of the classical GDEE is proposed, which implements the principle of probability preservation in space instead of time, making this approach suitable for the stochastic analysis of

finite element systems. The advantages of the FE Galerkin methods and in particular the SUPG over finite difference schemes, like the modified LW, which is the most frequently used method for the solution of the GDEE, are illustrated with numerical examples and explored further. The remaining of the paper is organized as follows: In the second section a concise review of the fundamentals of the PDEM is presented. In the third section a reformulation of the PDEM for general stochastic systems is introduced. In Sect. 4 the solution algorithm of the GDEE within the Galerkin framework, namely, the DG-FEM and SUPG formulations, is illustrated. Finally, in Sect. 5 the proposed methodologies are applied for the analysis of general stochastic systems and their applicability as well as performance over conventional LW methods is demonstrated and further discussed.

2 Fundamentals of the probability density evolution method

The principle of preservation of probability states that, the inflows, outflows and change in storage of probability in a control volume of the system must be in balance. This statement is mathematically expressed in the probability density evolution equation, namely the Fokker–Planck equation. It wasn't until the past few years, that a new perspective arose [4,24], that of the random event description and the above equation was re-derived, leading to a new family of GDEEs. To illustrate this concept, consider an n-dimensional stochastic dynamic system, whose equation of motion reads:

$$\mathbf{M}(\boldsymbol{\theta})\ddot{\mathbf{u}} + \mathbf{C}(\boldsymbol{\theta})\dot{\mathbf{u}} + \mathbf{f}(\boldsymbol{\theta}, \mathbf{u}) = \mathbf{F}(\boldsymbol{\theta}, t) \tag{1}$$

where $\mathbf{M}, \mathbf{C}, \mathbf{f}, \mathbf{F}$ are the mass and damping matrices, the restoring force vector and the excitation vector respectively; $\ddot{\mathbf{u}}$,$\dot{\mathbf{u}}$,$\mathbf{u}$ are the acceleration, velocity and displacement vectors of the structure; $\boldsymbol{\theta} = (\boldsymbol{\eta}, \boldsymbol{\zeta})$ the vector of all random parameters, with $\boldsymbol{\eta}$ being the vector of random parameters involved in the physical properties of the system and $\boldsymbol{\zeta}$ the vector of random parameters involved in the excitation.

Probing deeper into Eq. (1) reveals, that, besides the initial stochastic input for the system, which is fully contained in parameter $\boldsymbol{\theta}$, no other source of randomness enters or exits the system, as it evolves with time. This means, that the principle of preservation of probability holds, that is:

$$\frac{D}{Dt}\int_{\Omega_t \times \Omega_\theta} p_{\mathbf{u}\boldsymbol{\theta}}(\mathbf{u}, \boldsymbol{\theta}, t)\, \mathrm{d}\mathbf{u}\mathrm{d}\boldsymbol{\theta} = 0 \tag{2}$$

where, $\dfrac{D}{Dt}$ denotes the total or material derivative, $\Omega_t \times \Omega_\theta$ is any arbitrary domain in the augmented state space at time t, $\Omega_{\boldsymbol{\theta}}$ is the distribution range of the random vector $\boldsymbol{\theta}$ and $p_{\mathbf{u}\boldsymbol{\theta}}$ denotes the joint pdf of $(\mathbf{u}(t), \boldsymbol{\theta})$.

After a series of mathematical manipulations [24,26] Eq. (2) can be decoupled for each dof as

$$\int_{\Omega_0 \times \Omega_\theta} \left(\frac{\partial p_{\mathbf{u}\boldsymbol{\theta}}(\mathbf{u}, \boldsymbol{\theta}, t)}{\partial t} + \sum_{j=1}^{m} \dot{u}_j(\boldsymbol{\theta}, t) \frac{\partial p_{\mathbf{u}\boldsymbol{\theta}}(\mathbf{u}, \boldsymbol{\theta}, t)}{\partial u_j} \right) \mathrm{d}\mathbf{u}\mathrm{d}\boldsymbol{\theta} = 0 \tag{3}$$

where m is the total number of dof's. Since Eq. (3) holds for any arbitrary domain $\Omega_0 \times \Omega_\theta \in \Omega \times \Omega_{\boldsymbol{\theta}}$, then for any arbitrary $\Omega_\theta \in \Omega_{\boldsymbol{\theta}}$,

$$\int_{\Omega_\theta} \left(\frac{\partial p_{\mathbf{u}\boldsymbol{\theta}}(\mathbf{u}, \boldsymbol{\theta}, t)}{\partial t} + \sum_{j=1}^{m} \dot{u}_j(\boldsymbol{\theta}, t) \frac{\partial p_{\mathbf{u}\boldsymbol{\theta}}(\mathbf{u}, \boldsymbol{\theta}, t)}{\partial u_j} \right) \mathrm{d}\boldsymbol{\theta} = 0 \tag{4}$$

which results in the following partial differential equation:

$$\frac{\partial p_{\mathbf{u}\boldsymbol{\theta}}(\mathbf{u}, \boldsymbol{\theta}, t)}{\partial t} + \sum_{j=1}^{m} \dot{u}_j(\boldsymbol{\theta}, t) \frac{\partial p_{\mathbf{u}\boldsymbol{\theta}}(\mathbf{u}, \boldsymbol{\theta}, t)}{\partial u_j} = 0 \tag{5}$$

or in the case where m = 1, Eq. (5) reduces to

$$\frac{\partial p_{u\boldsymbol{\theta}}(u, \boldsymbol{\theta}, t)}{\partial t} + \dot{u}(\boldsymbol{\theta}, t) \frac{\partial p_{u\boldsymbol{\theta}}(u, \boldsymbol{\theta}, t)}{\partial u} = 0 \tag{6}$$

Equations (5), (6) (Eqs. (64b), (65) in [4]) are referred as the GDEEs and possess some significant advantages over the classical probability density evolution equations (Liouville, FP, etc.). More specifically, they reduce the high-dimensional stochastic differential equation, which can be unfeasible to solve numerically for problems with many dof's, into a series of one-dimensional deterministic partial differential equations. To solve the pde's we need the initial conditions for the problem, which for most of the cases are of the form:

$$p_{u\boldsymbol{\theta}}(u, \boldsymbol{\theta}, t)\ |_{t=t_0} = \delta(u - u_0)\, p_{\boldsymbol{\theta}}(\boldsymbol{\theta}) \tag{7}$$

Then, the solution to Eq. (6) leads to the marginal pdf of $u(t)$ as:

$$p_u(u, t) = \int_{\Omega_{\boldsymbol{\theta}}} p_{u\boldsymbol{\theta}}(u, \boldsymbol{\theta}, t)\mathrm{d}\boldsymbol{\theta} \tag{8}$$

Taking into account that Eq. (4) holds for any $\Omega_q \in \Omega_{\boldsymbol{\theta}}$,then if we partition Ω_θ into sub-domains, Ω_q's, $q = 1, 2, \ldots, n_{pt}$, such that $\Omega_i \cap \Omega_j = \emptyset, \forall i \neq j$ and $\cup_{q=1}^{n_{pt}} \Omega_q = \Omega_{\boldsymbol{\theta}}$, Eq. (6) becomes (for $m = 1$):

$$\int_{\Omega_q}\left(\frac{\partial p_{u\boldsymbol{\theta}}(u,\boldsymbol{\theta},t)}{\partial t}+\dot{u}(\boldsymbol{\theta},t)\frac{\partial p_{u\boldsymbol{\theta}}(u,\boldsymbol{\theta},t)}{\partial u}\right)\mathrm{d}\boldsymbol{\theta}=0,\quad q=1,2,\ldots,n_{pt} \tag{9}$$

The probability corresponding to the sub-domain Ω_q is then expressed as:

$$P_q=\int_{\Omega_q}p_{\boldsymbol{\theta}}(\boldsymbol{\theta})\mathrm{d}\boldsymbol{\theta},\quad q=1,2,\ldots,n_{pt} \tag{10}$$

If we denote

$$p_q(u,t)=\int_{\Omega_q}p_{u\boldsymbol{\theta}}(u,\boldsymbol{\theta},t)\mathrm{d}\boldsymbol{\theta},\quad q=1,2,\ldots,n_{pt} \tag{11}$$

then,

$$p(u,t)=\sum_{q=1}^{n_{pt}}p_q(u,t) \tag{12}$$

The procedure described above is referred to as the probability density evolution method and it is evident that the accuracy of this method depends solely on two parameters: (a) the partitioning of the probability domain and (b) the accurate solution of the corresponding pde's. For the latter, it has to be mentioned that, solving these pde's is not a trivial task, due to the fact that these equations are of the pure advection form with, in most cases, discontinuous initial conditions (shock-type). Therefore, the introduction of artificial dissipation (viscosity) is necessary to ensure the numerical stability of the solution, while adding too much dissipation will, as mentioned previously, result in a severe smearing of the solution.

3 PDEM for general stochastic systems

A reformulation of the GDEE for the analysis of general stochastic systems can be derived in a straightforward manner by following exactly the same steps deployed in the previous section. Consider the equation of equilibrium of a multi-degree-of freedom system

$$\mathbf{K}(\boldsymbol{\theta})\cdot\mathbf{u}=\mathbf{F}(\boldsymbol{\theta}) \tag{13}$$

where, $\mathbf{u}$ stands for the displacement vector along the dimension of one global degree of freedom. In this case our interest lies in finding the evolution of probability density function, along the material points or in other words, as a function of the position vector of the system, henceforth denoted as x in the case of one dimensional structures. The difference with the previous case is that, now, the rate or "velocity" of $\mathbf{u}$ is

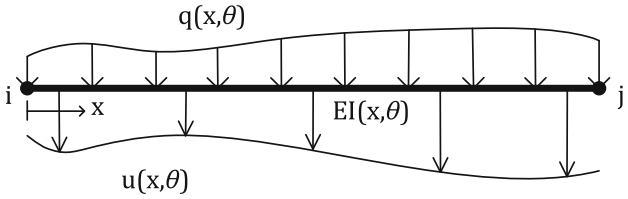

Fig. 1 Generic element with the randomness involved in the loading and the system parameters

with respect to the length of the structure and x replaces t in all the above equations.

Thus, we rewrite Eq. (6) as follows:

$$\frac{\partial p_{u\boldsymbol{\theta}}(u,\boldsymbol{\theta},x)}{\partial x}+\frac{du(\boldsymbol{\theta},x)}{dx}\frac{\partial p_{u\boldsymbol{\theta}}(u,\boldsymbol{\theta},x)}{\partial u}=0 \tag{14}$$

with initial conditions:

$$p_{u\boldsymbol{\theta}}(u,\boldsymbol{\theta},x)\mid_{x=x_0}=\delta(u-u_0)p_{\boldsymbol{\theta}}(\boldsymbol{\theta}) \tag{15}$$

Then the marginal pdf of $u(x)$ can be written as

$$p_u(u,x)=\int_{\Omega_{\boldsymbol{\theta}}}p_{u\boldsymbol{\theta}}(u,\boldsymbol{\theta},x)\mathrm{d}\boldsymbol{\theta} \tag{16}$$

For example, if we consider the generic element of Fig. 1 as a typical part of stochastic static system, it is obvious that the randomness involved in the loading q and the bending stiffness EI of the element, will lead to a random field $u(x)$, along the length of the element, which can be evaluated via Eq. (14) with the initial conditions expressed in Eq. (15). The initial conditions can be found at the edge nodes of the element. For instance, if we have fixed support at node i, then the displacement at this position will be zero with certain probability, and the initial condition reads: $p_{u\boldsymbol{\theta}}(u,\boldsymbol{\theta},x)\mid_{x=0}=\delta(u-0)p_{\boldsymbol{\theta}}(\boldsymbol{\theta})$.

4 Solution of the GDEE

The basic steps needed to solve the GDEE in Eq. (14), as proposed by Li and Chen [24], are outlined here. These steps are slightly modified to fit the case of general stochastic systems and are the following:

Step 1 Discretize the probability-assigned space and select representative point sets (random events) $\boldsymbol{\theta}_q=(\theta_{q,1},\theta_{q,2},\ldots,\theta_{q,s})$ with $q=1,2,\ldots,n_{pt}$, where n_{pt} is the cardinal number of the point set. To each point set determine the assigned probabilities P_q's via Eq. (10).
Step 2 Discretize the physical space into m partitions. For the prescribed $\boldsymbol{\theta}=\boldsymbol{\theta}_q$ solve the discretized deterministic equilibrium equation (Eq. (13)) with a standard FE

solver, to evaluate $\frac{du\left(\boldsymbol{\theta}_q, x_m\right)}{dx}$, where $x_m = m\Delta x$ $(m = 1, 2\ldots)$, Δx is the length step, $0 \leq x_m \leq L$, L being the length of the structure. Note that in case this partition does not coincide with the FE discretization, an extrapolation from the corresponding Gauss points is required.

Step 3 Introducing $\frac{du\left(u_{0,q}, \boldsymbol{\theta}_q, x_m\right)}{dx}$ into the GDEEs and taking into account the discretized version of Eq. (15), that is, $p_q(u, x) \mid_{x=x_0} = \delta(u - u_0) P_q$, solve Eq. (14) with a finite difference method, or a finite element method, as proposed in the next chapters, to obtain the numerical solution of $p_q(u, x)$.

Step 4 Repeat steps 2, 3 for $q = 1, 2, \ldots, n_{pt}$ and take the numerical integration in Eq. (16) to compute the numerical solution of $p_u(u, x)$.

It must be mentioned here that the strategy of selecting representative point sets at step 1 is of paramount importance to the efficiency of the method. Apart from the grid-type partitioning of the probability domain, many other strategies have been successfully employed, depending on the nature of the problem, that significantly reduce the computational cost of the method, such as the Number Theoretical Method [6,25], Tangent Sphere Method [3], Q-SPM [42], RQ-SPM [5] etc. In addition, solving the deterministic pde (Eq. (14)) at step 3 accurately and efficiently is a vital component of the whole procedure. When faced with this task, one quickly realizes that there is a wide range of methods to do so, including finite difference schemes, finite volume and finite element methods. The selection of the optimum scheme though isn't always an easy task. On the one hand, it depends on the problem under consideration (e.g. existence of steep gradients) as well as on the scheme chosen, as some schemes tend to be more dispersive and others more dissipative. From the three methods mentioned, finite difference schemes are the easiest to implement but they have certain drawbacks. For instance, central finite difference schemes lead to unstable solutions, while upwind methods suffer from overdissipation. In addition, finite difference schemes depend heavily upon the CFL condition, which poses a restriction on the incremental step of the method and as a consequence, an increase in the computational cost for the solution.

In this work we investigate two alternative to the widely used up to now LW schemes, based on Galerkin finite element approximations for solving Eq. (14). More specifically, we employ a time-marching discontinuous Galerkin scheme (DG-FEM) and the Streamline Upwind/Petrov Galerkin (SUPG) method. The motivation behind that, is the fact that Eq. (14) describes a conservation law and resembles the 1D hyperbolic advection equation. Both these methods have been successfully used for treating this type of pde's, each with its own merits [13,15]. Especially for the SUPG formulation, it's worth mentioning, that this method has the additional advantage of not being subjected to the CFL condition and, thus, leading to a more efficient solution scheme.

4.1 Space–time finite elements: the StreamlineUpwind/Petrov–Galerkin formulation

The StreamlineUpwind/Petrov–Galerkin concept (SUPG) was introduced by Hughes and Brooks [2,17], and the basic idea behind this method is to add numerical diffusion along the streamlines. In the above mentioned references, its application in the linear scalar advection equation is demonstrated. Since Eq. (14) resembles the advection equation, we can rewrite it in the following form:

$$\mathbf{w} \cdot \nabla p = 0 \tag{17}$$

where, $\mathbf{w} = (1, \alpha(x))$ the velocity field, $\alpha(x)$ is the flux $\frac{du(x)}{dx}$ and $\nabla p = (\partial p/\partial x,\ \partial p/\partial u)$. A finite element partition of the computational domain $\Omega = \Omega_u \times \Omega_x \subset R^2$ is denoted by $\{\Omega^e\}$ for $e = 1, 2, \ldots, N_{el}$. Since the domain is two dimensional, we can use quadrilateral elements to discretize Ω. Figure 2 illustrates this discretization of the physical domain with quadrilateral elements, where each dof corresponds to the probability at this position. The boundary conditions are Dirichlet on all of the boundary $\partial\Omega$, that is, $p = g$. According to [13] we can define the space of trial solutions as $\mathcal{V} = \{p | p \in \mathcal{H}^1(\Omega), p = g \text{ on } \partial\Omega\}$, where $\mathcal{H}^1 = \{p : \Omega \to R | p, \frac{\partial p}{\partial x}, \frac{\partial p}{\partial u} \in L_2(\Omega)\}$ is the

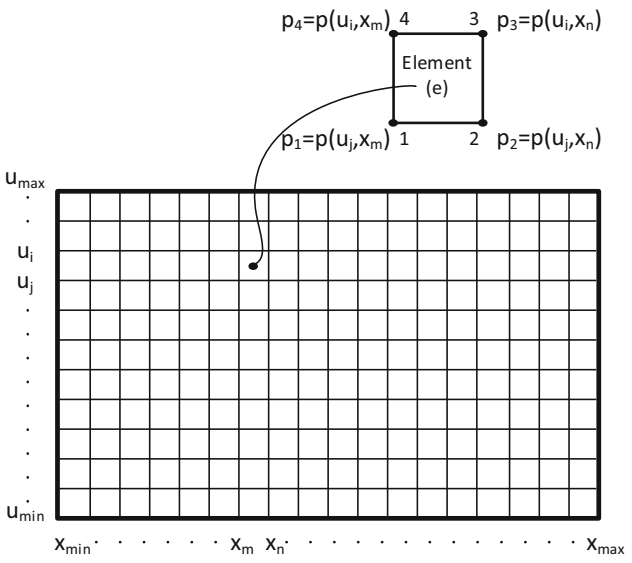

Fig. 2 Discretization of the physical domain into 4-noded quadrilateral finite elements with 1 degree of freedom per node, corresponding to the probability assigned to the displacement value and this position

Sobolev space and we also define the space $\mathcal{V}_0 = \{\psi | \psi \in \mathcal{H}^1(\Omega), \psi = 0 \text{ on } \partial\Omega\}$. The basic idea of Petrov–Galerkin approximation is to specify a weak formulation in which the space of test (weighting) functions is taken to be different than the space of the trial solutions.More specifically, the test space is the space spanned by functions of the form:

$$\tilde{\psi} = \psi + \tau \mathbf{w} \nabla \psi \tag{18}$$

where $\psi \in \mathcal{V}_0$ is the Galerkin-type weighting function and τ is a coefficient, which for each element e is given by the following expression [2]:

$$\tau_e = \frac{\mathsf{a}\lambda_e}{2|\mathbf{w}_e|} \tag{19}$$

In the above expression λ_e is the characteristic length of the e element given by $\lambda_e = min\left(\frac{\lambda_x}{cos\vartheta}, \frac{\lambda_u}{sin\vartheta}\right)$ with λ_x, λ_u being the rectangle's lengths in x and u direction, respectively, and $\vartheta = arctan\left(\left|\frac{w_u}{w_x}\right|\right)$. In the following equations we will use the subscript h to refer to the discrete finite element problem. The weak form of Eq. (17) can be written as

$$\int_\Omega \psi^h \mathbf{w} \nabla p^h d\Omega + \sum_{e=1}^{n_{el}} \int_{\Omega_e} \tau \mathbf{w} \nabla \psi^h \mathbf{w} \nabla p^h d\Omega_e = 0 \tag{20}$$

In Eq. (19) a is the upwind function, which depends on the element Peclet number Pe ($Pe = \infty$ for pure advection). The expression $\mathsf{a} = coth(Pe) - \frac{1}{Pe}$, with a being equal to 1 in our case, can be used.

In order to further enhance the accuracy of the method, we add a discontinuity capturing term in Eq. (20) based on the methodology presented in [17]. Then, Eq. (20) is rewritten as follows:

$$\int_\Omega \psi^h \mathbf{w} \nabla p^h d\Omega + \sum_{e=1}^{n_{el}} \int_{\Omega_e} \tau_1 \mathbf{w} \nabla \psi^h \mathbf{w} \nabla p^h d\Omega_e + \sum_{e=1}^{n_{el}} \int_{\Omega_e} \tau_2 \mathbf{w} \nabla \psi^h \mathbf{w}_\parallel \nabla p^h d\Omega_e = 0 \tag{21}$$

where, $\mathbf{w}_\parallel$ denotes the projection of $\mathbf{w}$ onto ∇p^h, that is,

$$\mathbf{w}_\parallel = \begin{cases} \dfrac{\mathbf{w}\nabla p^h}{|\nabla p^h|_2^2}, & \text{if } \nabla p^h \neq 0 \\ 0, & \text{if } \nabla p^h = 0 \end{cases} \tag{22}$$

According to [17], $\tau_1 = \tau$ and $\tau_2 = max\left(0, \tau_\parallel - \tau\right)$, where $\tau_\parallel$ is computed as indicated in Eq. (19), but using $\mathbf{w}_\parallel$ instead of $\mathbf{w}$. In a matrix notation, Eq. (21) can be rewritten as:

$$\mathcal{K}\mathbf{p} = 0 \tag{23}$$

where,

$$\mathcal{K} = \mathcal{A} + \mathcal{S} \tag{24}$$

$$\mathcal{K}_{ij} = \mathcal{A}_{ij} + \mathcal{S}_{ij} \tag{25}$$

$$\mathcal{A}_{ij} = \int_\Omega \left(\mathbf{w}\nabla\varphi_j\right)\varphi_i \tag{26}$$

$$\mathcal{S}_{ij} = \sum_{e=1}^{n_{el}} \int_{\Omega_e} \tau_1 \mathbf{w}\nabla\varphi_j \mathbf{w}\nabla\varphi_i + \sum_{e=1}^{n_{el}} \int_{\Omega_e} \tau_2 \mathbf{w}\nabla\varphi_j \mathbf{w}_\parallel \nabla\varphi_i \tag{27}$$

and $\{\varphi\}$ is the basis that spans the functional spaces.

4.2 Discontinuous Galerkin finite element method (DG-FEM)

The DG method is a robust and compact finite element projection method, well suited for dealing with partial differential equations describing conservations laws (e.g. advection equation). It can be seen as a combination of the finite element method and the finite volume method, taking advantages from both. An important distinction between the DG method and the usual finite-element method is that in the DG-FEM the resulting equations are local to the generating element and the coupling of the elements is achieved using the appropriate numerical flux across the elements. Thus, each element may be thought of as a separate entity that merely needs to obtain some boundary data from its neighbours and no global linear or nonlinear systems need to be solved. Moreover, a numerical flux can be chosen to be more or less dissipative, depending on the problem under consideration.

Consider the following equation representing a GDEE.

$$\frac{\partial p_q(u,x)}{\partial x} + \alpha_q(x)\frac{\partial p_q(u,x)}{\partial u} = 0, \quad \text{for } q = 1, 2, \ldots n_{pt} \tag{28}$$

under the initial condition:

$$p_q(u,0) = p_{q,0}(u) \tag{29}$$

where, $\alpha_q(x)$ is the flux $\frac{du_q(x)}{dx}$, $u \in [u_{min}, u_{max}] = \Omega_u$ and $0 \leq x \leq L$, with L being the length under consideration in the stochastic system. Without introducing any ambiguities, we will omit the subscript q in the above expression and introduce the subscript h to refer to the discrete solution. Partitioning the domain Ω_u by K non-overlapping elements $u \in \left[u_l^k, u_r^k\right] = D^k$ such that

$$\Omega_u \cong \Omega_u^h = \bigcup_{k=1}^{K} D^k \tag{30}$$

where u_l^k and u_r^k are the left and right displacements of element k, then on each of these elements the local solution can be expressed as a polynomial of order $N = N_p - 1$.

$$u \in D^k : p_h^k(u,x) = \sum_{i=1}^{N_p} p_h^k\left(u_i^k, x\right) l_i^k(u) \tag{31}$$

where $l_i^k(u)$ are the interpolating Lagrange polynomials and $p_h^k\left(u_i^k, x\right)$ refers to the nodal values. The global solution $p(u,x)$ is then assumed to be approximated by the N-th order polynomial approximation $p_h(u,x)$, that is:

$$p(u,x) \cong p_h(u,x) = \bigoplus_{k=1}^{K} p_h^k(u,x) \tag{32}$$

defined as the direct sum of the K local polynomial solutions $p_h^k(u,x)$.

Following the procedure described in [15] a strong DG-form of (28) for each element k can be written in matrix notation as follows

$$\boldsymbol{M}^k \frac{d}{dx}\boldsymbol{p}_h^k + \boldsymbol{S}^k \alpha \boldsymbol{p}_h^k = \left[\boldsymbol{l}^k(u)(\alpha p_h^k - f^\star)\right]_{u_l^k}^{u_r^k} \tag{33}$$

where $\boldsymbol{M}^k$ and $\boldsymbol{S}^k$ are the element's mass and stiffness matrices respectively. More specifically:

$$M_{ij}^k = \int_{D_k} l_i^k(u) l_j^k(u) du \tag{34}$$

$$S_{ij}^k = \int_{D_k} l_i^k(u) \frac{dl_j^k(u)}{du} du \tag{35}$$

and $f^\star$ is a suitably chosen numerical flux, which controls the information entering and exiting the element. In our calculations we used the monotone Lax–Friedrichs flux [23,30], while for the integration with respect to x we used a third-order three-stage Runge–Kutta scheme [15]. In addition, in order to prevent the well known oscillations appearing in the DG-FEM solution, the DG scheme was equipped with the MUSCL (Monotone Upstream-centered Scheme for Conservations Laws) slope limiter [23].

It must be mentioned here, that the stability of the DG method is controlled by the CFL condition, which generally depends on the selection of numerical flux, the order of elements used and the finite difference scheme employed. In our case, the inequality $\Delta x \leq \frac{1}{|\alpha|}\Delta u$ poses a reasonable bound for the choice of Δu and Δx.

4.3 Lax–Wendroff finite difference method with TVD scheme

A modified version of the LW scheme proposed in [24] is also used for solving Eq. (14), in order to compare its efficiency and accuracy to the previously described SUPG and DG methods, equipped with flux limiters to ensure the non-negativity of the solution, imposed by the nature of the pdf. More specifically, if we denote $p_u(u_j, \boldsymbol{\theta}, x_m) = p_{j,m}$, then,as described in Eq. (29) of reference [24], Eq. (14) is discretized into the form

$$\begin{aligned} p_{j,m+1} = p_{j,m} - r_L\Big[&\frac{1}{2}(g_m + |g_m|)(p_{j,m} - p_{j-1,m}) \\ &+ \frac{1}{2}(g_m - |g_m|)(p_{j+1,m} - p_{j,m})\Big] - \frac{1}{2}(1 - |r_L g_m|) \\ &\times |r_L g_m|\Big[\chi\left(r^+_{j+\frac{1}{2}}, r^-_{j+\frac{1}{2}}\right)(p_{j+1,m} - p_{j,m}) \\ &- \chi\left(r^+_{j-\frac{1}{2}}, r^-_{j-\frac{1}{2}}\right)(p_{j,m} - p_{j-1,m})\Big] \end{aligned} \tag{36}$$

where $x_m = m \cdot \Delta x$ and Δx is the length step in the difference method; $r_L = \frac{\Delta x}{\Delta u}$ is the lattice ratio; Also,

$$\begin{aligned} r^+_{j+\frac{1}{2}} &= \frac{p_{j+2,m} - p_{j+1,m}}{p_{j+1,m} - p_{j,m}}, \quad r^-_{j+\frac{1}{2}} = \frac{p_{j,m} - p_{j-1,m}}{p_{j+1,m} - p_{j,m}} \\ r^+_{j-\frac{1}{2}} &= \frac{p_{j+1,m} - p_{j,m}}{p_{j,m} - p_{j-1,m}}, \quad r^-_{j-\frac{1}{2}} = \frac{p_{j-1,m} - p_{j-2,m}}{p_{j,m} - p_{j-1,m}} \end{aligned} \tag{37}$$

The coefficients g_m take the value

$$g_m = \frac{1}{2}\left(\frac{du(\boldsymbol{\theta}, x_{m-1})}{dx} + \frac{du(\boldsymbol{\theta}, x_m)}{dx}\right) \tag{38}$$

$\chi(r^+, r^-)$ is the flux limiter, which is constructed based on the Roe-Sweby flux limiter

$$\chi_{sb}(r^-) = max(0, min(2r^-, 1), min(r^-, 2)) \tag{39}$$

and

$$\chi(r^+, r^-) = H(-g_m)\chi_{sb}(r^+) + H(g_m)\chi_{sb}(r^-) \tag{40}$$

with H being the Heaviside function.

A necessary (but not sufficient) condition for the stability of the scheme is the CFL condition, which for Eq. (36) reads: $|r_L g_m| \leq 1$.

5 Numerical examples

Example 1 Portal frame.

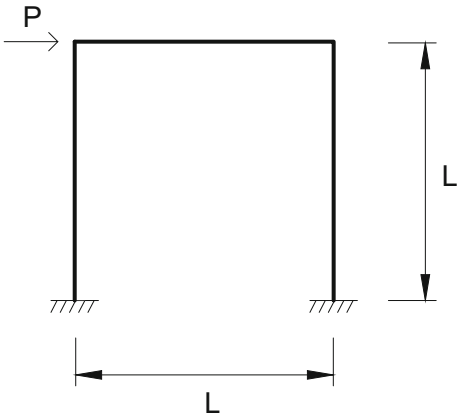

Fig. 3 1-story stochastic structure

The simple example of the portal frame of Fig. 3 is chosen first, in order to test the accuracy of the proposed methodologies. For this frame of length and height equal to $L = 5$ m, a HEB 220 [35] cross-section is assigned to all its members. The random parameters considered are the modulus of elasticity E and the horizontal force P, which are assumed to follow the gaussian distribution with mean $\bar{E} = 21000\ \frac{\text{kN}}{\text{cm}^2}$, coefficient of variation $COV_E = 0.10$, mean $\bar{P} = 30kN$ and $COV_P = 0.15$. In this case, our interest lies in finding the evolution of the probability density function of the horizontal displacement u along the length of each member of the frame. Geometric and material nonlinearities are included in the model. For the material nonlinearity an elastic-perfectly plastic constitutive law is assummed with a yield stress of $F_y = 355$ MPa. In the absence of an analytical solution to our problem the results of a large number of Monte Carlo simulations were considered as the 'exact solution' for comparison purposes.

Depicted in the following figures are the mean value and variance along the length of the path, the evolution of the pdf $p(u, x)$, and typical pdf profiles at certain positions (snapshots), computed with the various proposed methodologies and the brute force Monte Carlo Simulation (MCS). Figure 4 presents a comparison in the mean value between the MCS and the three different approaches, SUPG, LW and DG-FEM, respectively. We notice a perfect match in all cases. The same comparison in terms of variance is depicted in Fig. 5 for two different grids used to discretize the domain $\Omega_u \times \Omega_x$, namely, grid A with 150×600 elements and grid B with 450×1500. Figure 5a, b presents the results for grid A and grid B, respectively. It can be seen in these figures that only SUPG has converged to the MC solution with the coarse grid A, while the DG and LW require a more dense mesh to achieve the same accuracy. The reason behind this is excessive dissipation observed (see Fig. 7) in LW and DG-FEM, which leads to overly diffuse and spread out solutions.

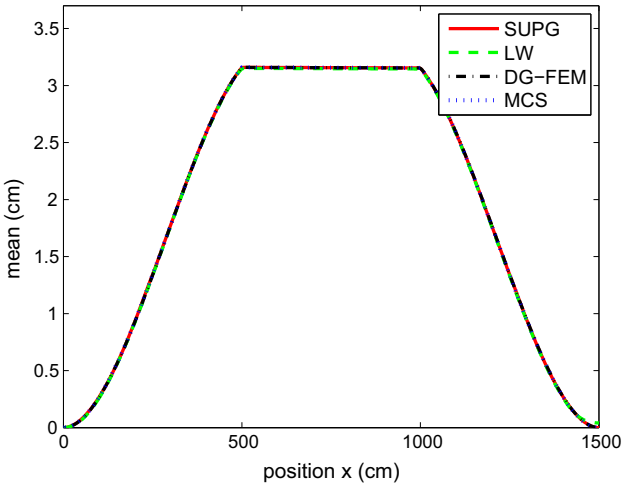

Fig. 4 Comparison in mean value between the SUPG, the modified LW and the DG-FEM for a 150 × 600 grid with brute force Monte Carlo simulation. (Color figure online)

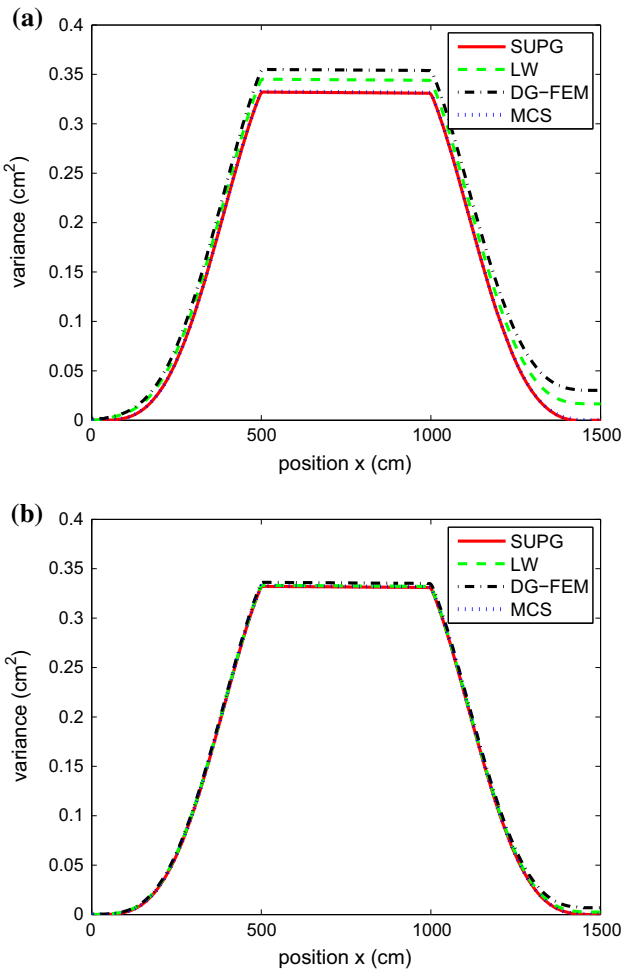

Fig. 5 Comparison in variance between the SUPG, the modified LW and the DG-FEM for a **a** 150 × 600 grid and **b** 450 × 1500 grid with brute force Monte Carlo simulation. (Color figure online)

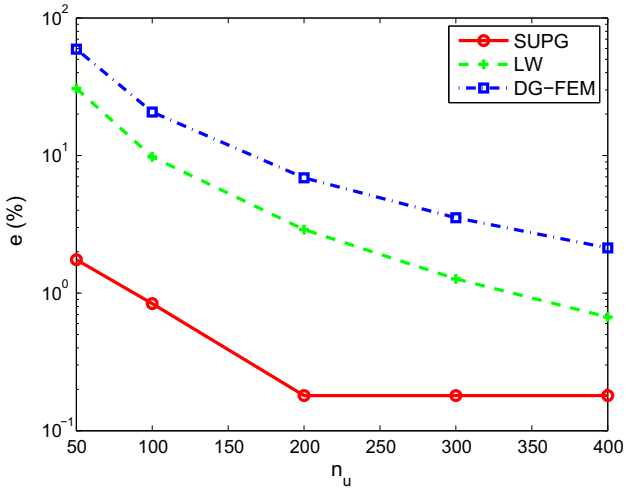

Fig. 6 Convergence error (%) in variance as a function of the number of elements in the Ω_u domain for the SUPG, the modified LW and the DG-FEM. (Color figure online)

Nevertheless, in Fig. 5b it becomes apparent, that a finer grid tends to significantly improve the results. Besides that, from Figs. 4, 5 it is also worth noticing that the mean value and the variability of the horizontal displacement u, remains invariant along the length of the beam, since the term $\frac{du}{dx}$ in Eq. (14) becomes equal to zero and therefore, $p(u, x)$ becomes constant. The faster convergence of SUPG is further illustrated in the convergence study of Fig. 6 from which, it is evident that SUPG has the highest convergence rate among the three methods and achieves a considerably smaller error for the same number of elements in the Ω_u domain. The corresponding mesh sizes were selected as the minimum ones that satisfy the CFL condition for the LW and DG-FEM, in order for the solution to be stable. This CFL imposed restriction can be avoided, however, if we choose to employ the SUPG method, in which the discretization on Ω_u can be refined indepedently of the Ω_x discretization. This advantage of the SUPG will be illustrated in more detail in the next example.

In Fig. 7 the evolution of $p(u, x)$ along each position of the structure is presented, where the 450×1500 grid was applied in all cases. In this figure it is demonstrated how the initial probability "flows" through the physical domain for (a) the MCS method, (b) the SUPG formulation, (c) the

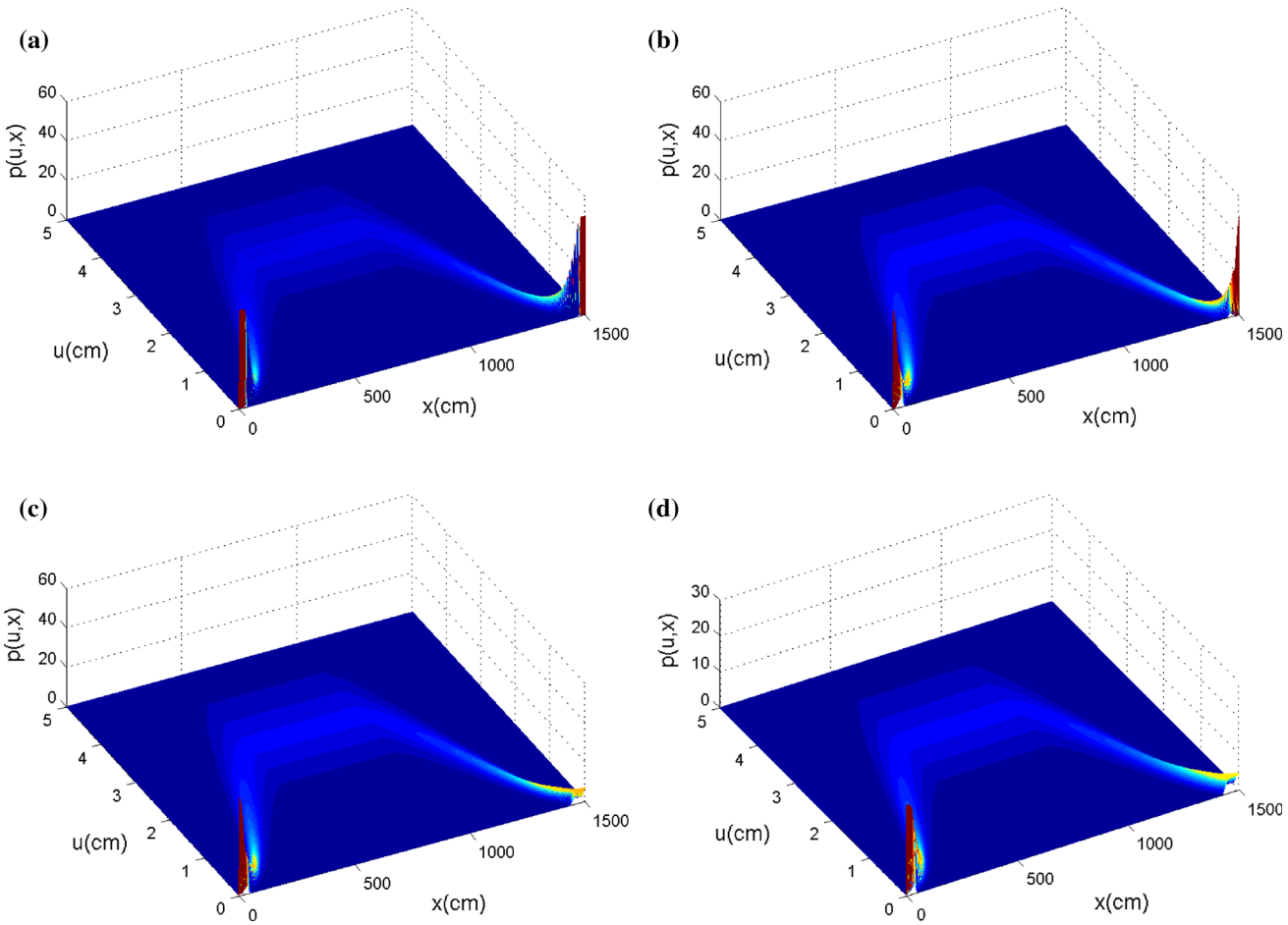

Fig. 7 Evolution of the probability density function $p(u, x)$ for **a** the Monte Carlo Simulation, **b** the SUPG, **c** the modified LW and **d** the DG-FEM. (Color figure online)

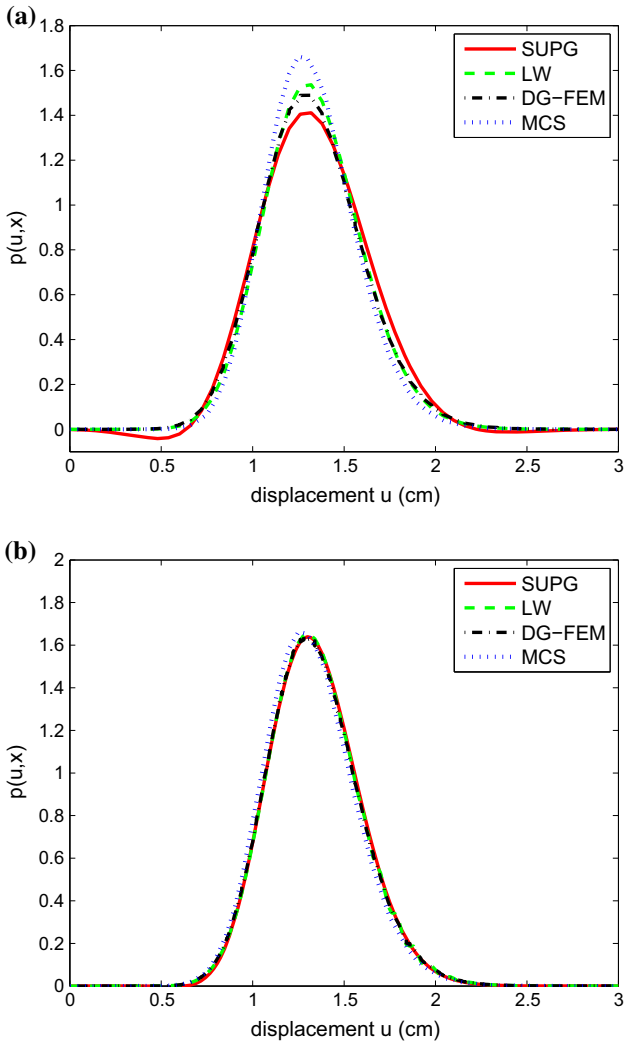

Fig. 8 PDF profiles at x = 2.50 m for the SUPG, the modified LW and the DG-FEM for a **a** 150 × 600 grid and **b** 450 × 1500 grid versus brute force Monte Carlo. (Color figure online)

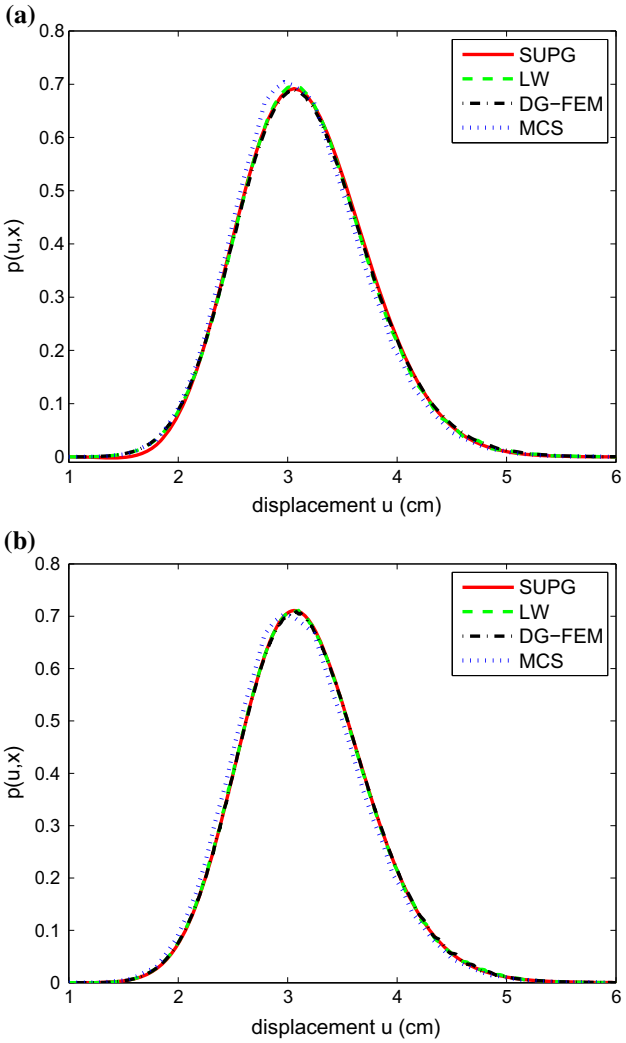

Fig. 9 PDF profiles at x = 7.50 m for the SUPG, the modified LW and the DG-FEM for a **a** 150 × 600 grid and **b** 450 × 1500 grid versus brute force Monte Carlo. (Color figure online)

modified Lax Wendroff scheme and (d) the DG-FEM. The x-axis denotes the position of the structure, with x ranging from 0 to $3L$, the y-axis denotes the possible values of the horizontal displacement u and the z-axis the pdf values $p(u, x)$ in each position. An intersection with a vertical plane parallel to the y-axis will give the pdf profile at this position. Due to the geometry and boundary conditions of the structure, a symmetrical profile of the evolution of the pdf is expected, and also, in the locations of the supports ($x = 0$ and $x = 3L$) all the probability should be lumped at the certain event of a zero displacement. From these figures it is obvious, that only the SUPG method equipped with the shock capturing terms in Eq. (21) can capture this symmetry. The DG-FEM formulation and the modified LW scheme fail to do so, due to the artificial dissipation added in these methods. Even with an increase in the number of elements in the grid, the probability at this boundary could not be accurately captured.

Finally, Figs. 8, 9 plot the pdf profiles at the positions $x = 2.50$ and $x = 7.50$ m, respectively, for the two mesh sizes mentioned earlier. Inspection of these figures reveals some very useful conclusions for each method. Specifically, SUPG has the disadvantage of not being a monotone method and thus, developing an undershoot at the base of the advancing discontinuities, which results in negative pdf values in their neighbourhood. This conclusion is more obvious in Fig. 8a, which is closer to the boundaries of the structure, and less in Fig. 9a. This problem, though, can be significantly ameliorated by considering a denser mesh, which is able to resolve the discontinuities [16]. Indeed, from Figs. 8b, 9b where a denser mesh (450 × 1500) is applied, a significant reduction of the undershoot associated with SUPG can be observed. On

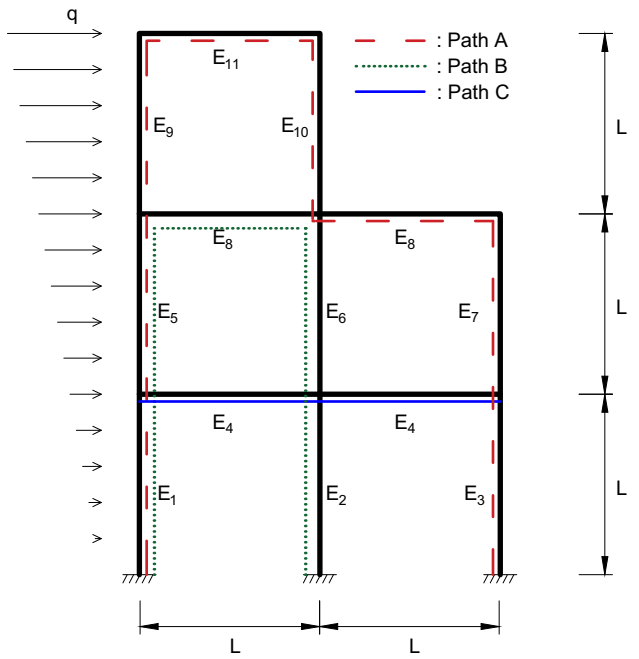

Fig. 10 3-story, 2-bay stochastic frame structure. (Color figure online)

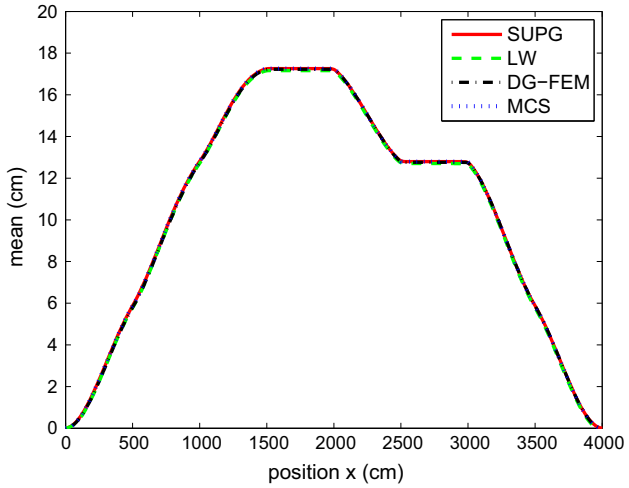

Fig. 11 Comparison in mean value between the SUPG, the modified LW and the DG-FEM with brute force Monte Carlo simulation. (Color figure online)

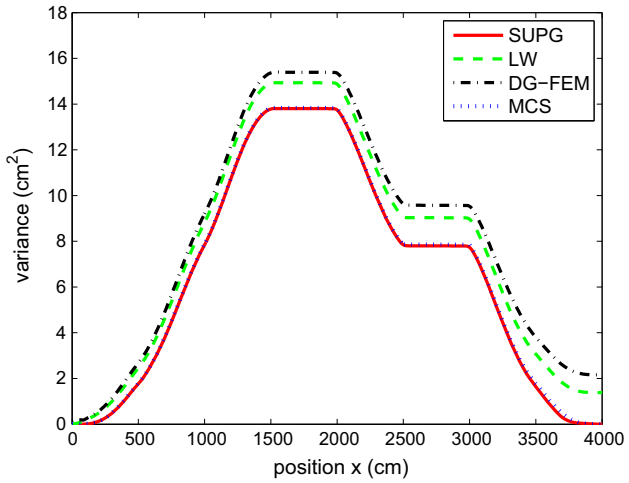

Fig. 12 Comparison in variance between the SUPG, the modified LW and the DG-FEM with brute force Monte Carlo simulation. (Color figure online)

the other hand, the LW and DG-FEM possess the TVD property and thus the non-negativity of the solution is ensured. From Figs. 8a, 9a however, we observe that both these methods suffer from a noticeable "smearing" in the solution profile due to the excess dissipation added in the schemes. Again, the situation can be improved by using a finer grid (Figs. 8b, 9b).

Example 2 Static response of a two-bay, three-story frame.

A more realistic case which is the 3-storey, 2-bay structure of Fig. 10 is considered as the second test case. In this more complex structure, the path, along which we estimate the evolution of probability is not unique. In Fig. 10 the red (dashed) line denotes the path we chose to investigate, but alternative paths can be chosen as well, provided that the initial conditions are well defined. Initial conditions are not necessarily defined at some support of the structure. For instance if we have already evaluated the pdf at the upper left node of the first story, then we can proceed along the path denoted with the blue (solid) line in Fig. 10 defining as initial conditions the calculated pdf at this point. The loading, the moduli of elasticity of each column, the beams of each floor and the yielding stresses of the materials in each storey are considered as random parameters, with properties the ones presented in Table 1. The partitioning of the corresponding probability domain plays an important role in the efficiency of the method and for this reason we chose to employ the Rotational Quasi-Symmetric Point Method (RQ-SPM) method in order to determine the representative point sets of the domain. Implementation aspects of the RQ-SPM can be found in [5]. Only 286 representative point sets are required for the method to achieve a partioning of the probability domain with an error of 3.58 %, which can be considered as small enough. These sets can also be found in [5]. As in the previous example, we

Table 1 Random parameters of the structure

	E_1-E_4	E_5-E_8	E_9-E_{11}	f_{y_1}	f_{y_2}	f_{y_3}	q
Mean	210 GPa	200 GPa	190 GPa	425 MPa	355 MPa	275 MPa	10 kN/m^2
COV	0.2	0.2	0.2	0.2	0.2	0.2	0.2

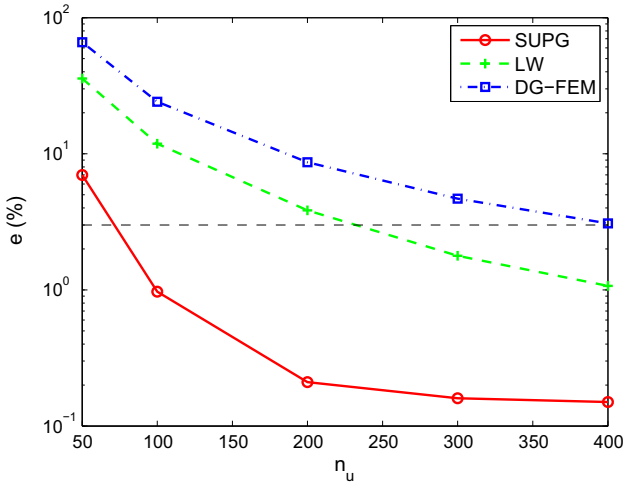

Fig. 13 Convergence error (%) in variance as a function of the number of elements in the Ω_u domain for the SUPG, the modified LW and the DG-FEM cases. (Color figure online)

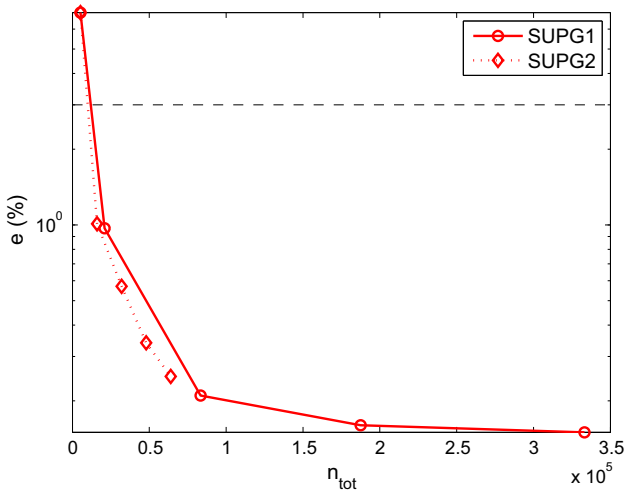

Fig. 14 Convergenve error (%) in variance as a function of the total number of degrees of freedom n_{tot} in the $\Omega_u \times \Omega_x$ domain for the SUPG1 and SUPG2 cases. (Color figure online)

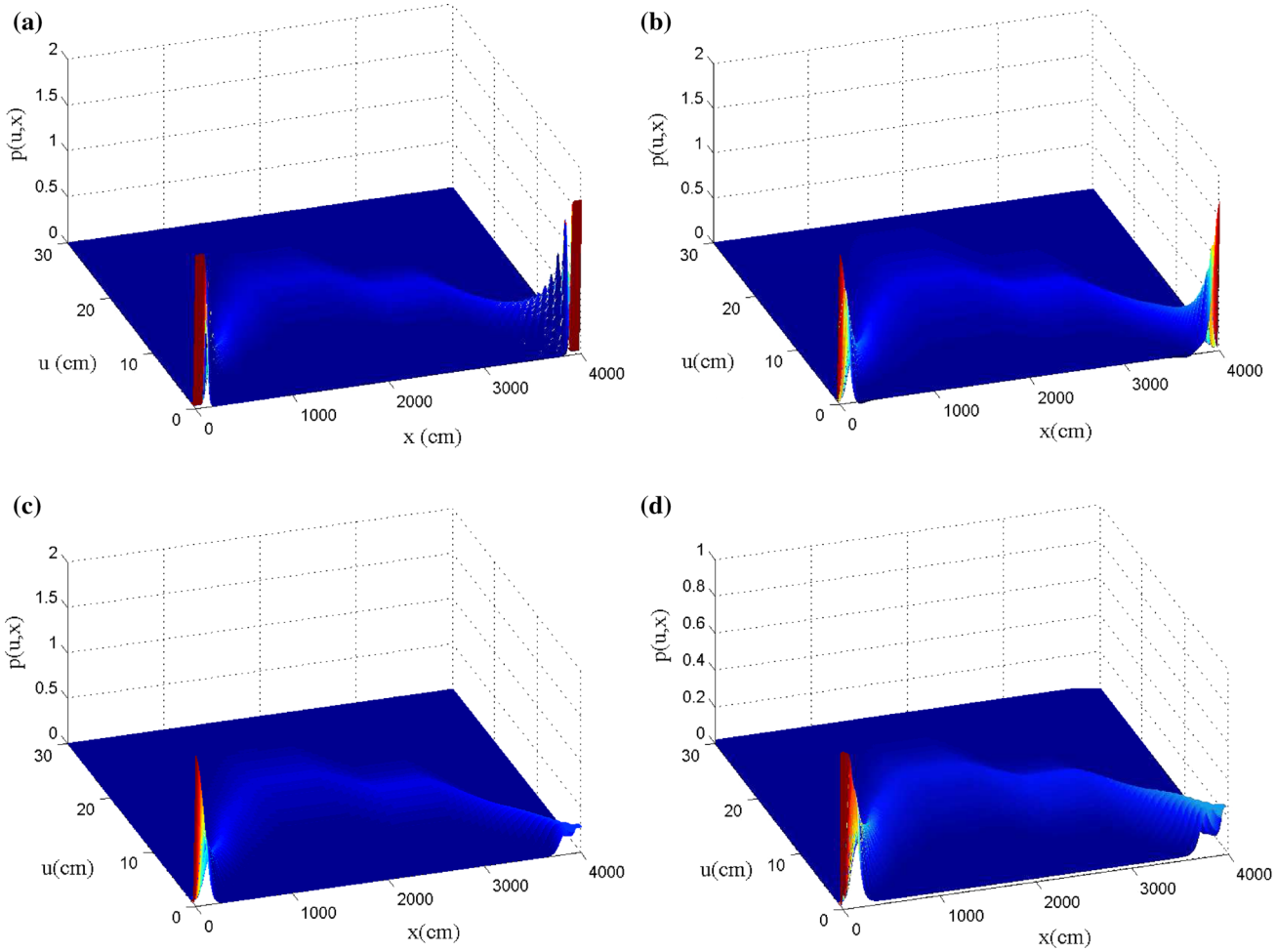

Fig. 15 Evolution of the probability density function $p(u, x)$ for **a** the Monte Carlo Simulation, **b** the SUPG, **c** the modified LW and **d** the DG-FEM. (Color figure online)

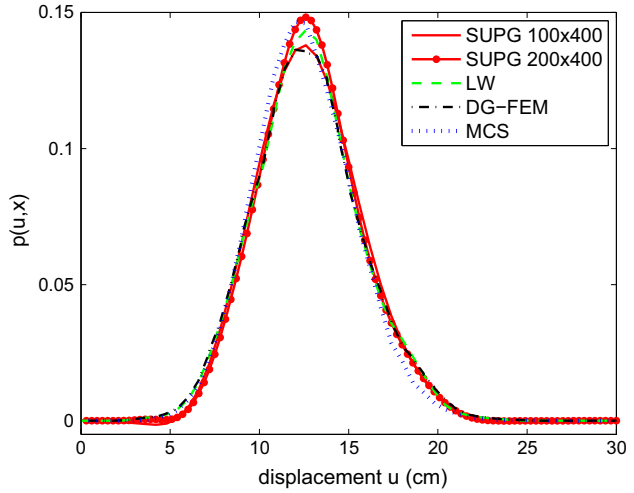

Fig. 16 PDF profiles at x = 10.00 m for SUPG 100 × 400, SUPG 200 × 400, modified LW and DG-FEM versus brute force Monte Carlo. (Color figure online)

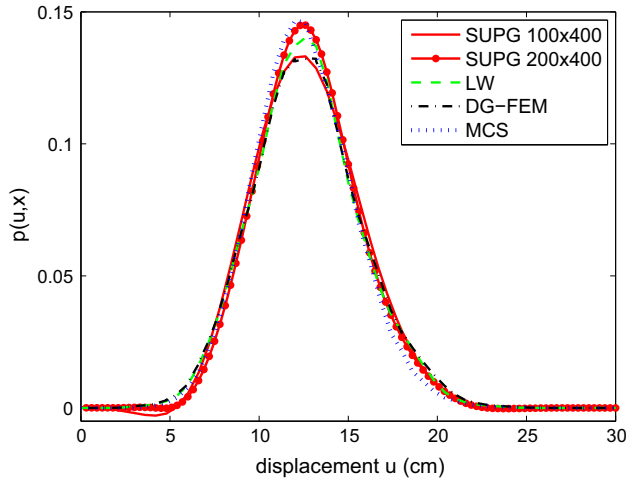

Fig. 17 PDF profiles at x = 30.00 m for SUPG 100 × 400, SUPG 200 × 400, modified LW and DG-FEM versus brute force Monte Carlo. (Color figure online)

used HEB 220 for all section types of the frame members, all having a length of $L = 5$ m. Geometrical and material nonlinearities were also included in the model.

Figures 11 and 12 present the mean and variance as a function of the position along the selected path, calculated with all aforementioned methodologies, for a 100×400 grid. From these figures it is apparent that, as in the previous example, in terms of mean all methods provide excellent results, while in terms of variance SUPG provides the most accurate results. The convergence rates in variance for each method are also investigated and the results are depicted in Fig. 13. Again, the superiority of SUPG is evident. As mentioned previously, another advantage of the SUPG method, that has not been exploited yet, is the fact that this method is not restricted under the CFL condition, like the other two methods. Therefore, the Ω_x domain in SUPG can be discretized in as many elements as necessary to obtain an accurate solution indepedently of the Ω_u disretization. In the LW and DG-FEM cases the number of elements in Ω_x must obey the CFL condition and thus they should be significantly increased leading to a more expensive mesh. This advantage of the SUPG is demonstrated in Fig. 14, which plots the convergence error in variance against the total number of elements in the domain for two cases, namely 'SUPG1' and 'SUPG2'. In both cases the same number of elements for the discretization of Ω_u is used, but in the former case ('SUPG1') the Ω_x is discretized in as many elements as required by the CFL condition, while for the latter ('SUPG2') a smaller number is used, namely 160 elements for all analyses. From this figure, it can be observed that SUPG can achieve almost the same level of accuracy for a significantly coarser mesh with the consequent reduction in the computational burden.

Table 2 Computational cost for each method

	Solving one pde	Number of analyses	Total CPU time
SUPG	0.289 s	286	82.709 s
Lax–Wedroff	1.829 s	286	523.032 s
DG-FEM	1.904 s	286	544.663 s

Figure 15 presents the evolution of the pdf along the length of the chosen path for the (a) MCS, (b) SUPG, (c) LW and (d) DG-FEM formulation. Again, it is apparent that only the SUPG can capture accurately the probability at the end of the domain. As in the previous example, the variability of the horizontal response remains constant along the beams, a result that agrees with the physical interpretation. In Figs. 16 and 17 the pdf profiles at the positions $x = 10.0$ and $x = 30.0$ m respectively, are presented. In all cases we used the same 100×400 grid, expect for the SUPG case where we also used a 200×400 grid for comparison purposes. The results are of fair accuracy but some weaknesses for each method can also be reported. More specifically, SUPG allows the pdf to take negative values, while LW and DG-FEM produce more "smeared" profiles. For the SUPG case, in particular, this problem could be ameliorated by considering a finer grid and this becomes evident from the results of the SUPG case with the denser mesh, where a noticeable improvement can be reported.

Finally, an assessment of the performance of the proposed methodologies is attempted here on the basis of computing time required to reach the solution. In order for the comparison to be fair we used the exact grid that gives an error of 3 % in variance for each method. More specifically, we considered a 84×160, a 241×513 and a 400×851 grid for SUPG, LW and DG-FEM respectively. The computational cost for each method in terms of total CPU time is illus-

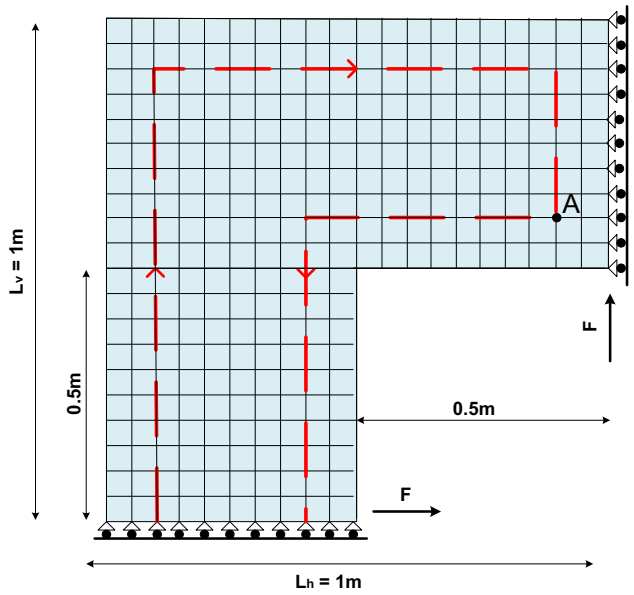

Fig. 18 L-shaped plane stress problem

Table 3 Random parameters of the structure

	E	F	ν
Mean	21 GPa	5000 kN	0.3
COV	0.2	0.2	0.2

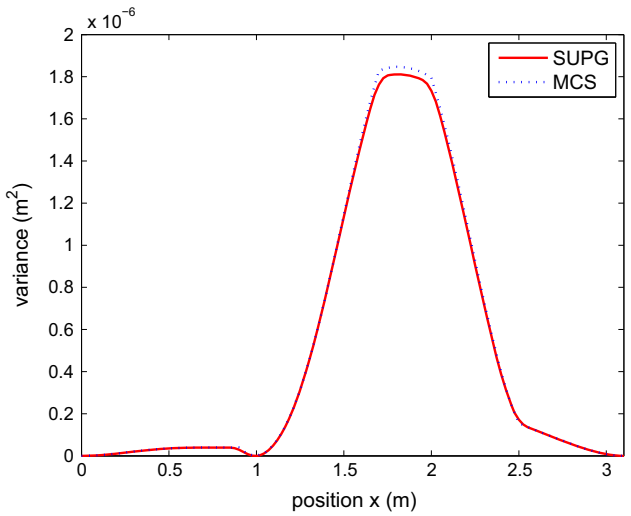

Fig. 19 Comparison in variance between SUPG and brute force Monte Carlo simulation. (Color figure online)

trated in Table 2. From this table it is apparent that the SUPG method is the most efficient choice, while the LW and the DG-FEM require six to seven times the cost of SUPG.

Example 3 Plane stress problem.

Finally, the L-shaped plane stress problem of Fig. 18 is considered, in order to demonstrate the applicability of the proposed methodology to general stochastic finite element

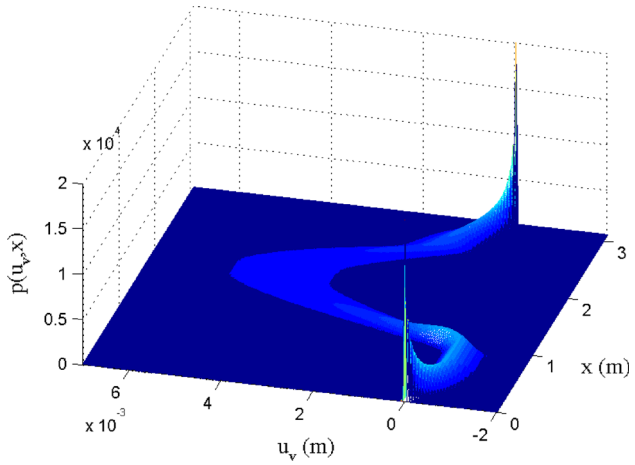

Fig. 20 Evolution of the probability density function of the vertical displacement $p(u_v, x)$ obtained by the PDEM with the SUPG formulation

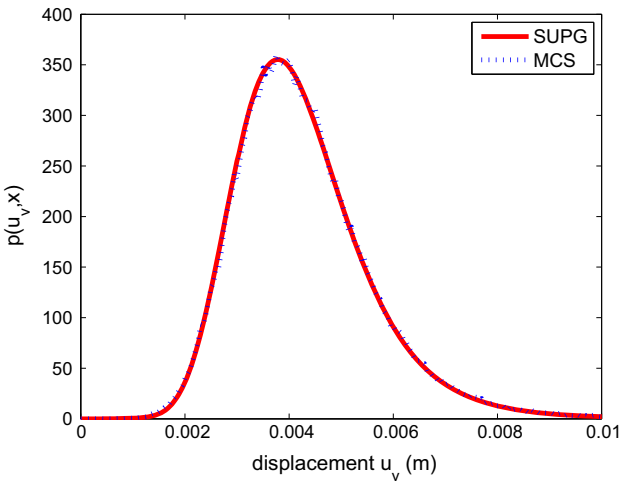

Fig. 21 PDF profiles at x = 2.0 m for the SUPG and brute force Monte Carlo simulation. (Color figure online)

systems. In this example the modulus of elasticity E, the forces F and the Poisson ratio ν are assumed random and follow a Gaussian distribution with properties the ones presented in Table 3. For the solution of the physical problem, the plate is discretized into 340 quadrilateral finite elements resulting in 682 dof's. In this case, our interest lies in estimating the evolution of the pdf of the vertical displacement u_v. It should be noted here that, despite the fact that the problem is two-dimensional, the one-dimensional version of the GDEE in Eq. (14) can be implemented in the same way, that it was implemented in the previous Example 2. Therefore, a path has to be selected at first, in order to apply the proposed methodology. Such a path is depicted with the red (dashed) line in Fig. 18 and its total length is 3.1 m.

Figure 19 plots the variance of the vertical displacement along the selected path computed with the PDEM with SUPG and MCS. As shown in this figure, the results are in close

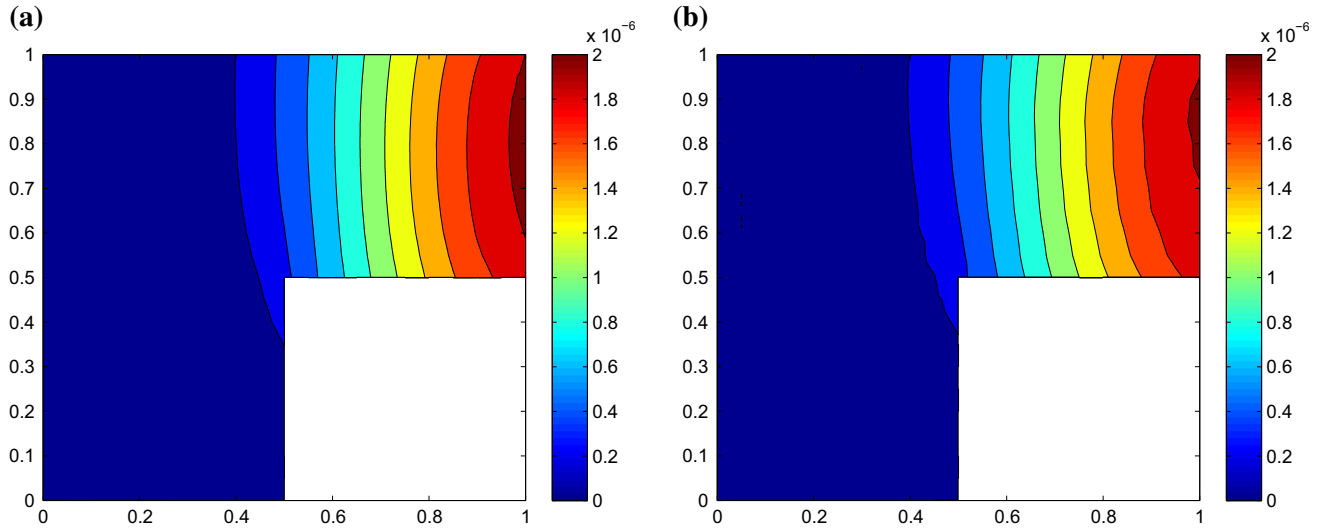

Fig. 22 Contour plots of variance for a the Monte Carlo Simulation and b the SUPG. **a** Monte Carlo Simulation. **b** StreamlineUpwind/Petrov Galerkin. (Color figure online)

agreement. Figure 20 presents the evolution of the pdf of the vertical displacement $p(u_v, x)$ along the length of the selected path for the SUPG. It becomes obvious that SUPG indeed manages to capture accurately the probabilistic information at the boundaries. An intersection with a vertical plane parallel to the u_v-axis at position $x = 2.0$ m, which corresponds to node A with coordinates (0.9, 0.6), will give the pdf profile of the vertical displacement at this position, as illustrated in Fig. 21. Again the results between MCS and PDEM are in almost perfect match. Lastly, instead of the chosen path we could consider a path that runs through all the nodes of the problem and estimate the complete probabilistic characteristics of the vertical displacement. In this case though, boundary conditions would have to be imposed not only at the edges of the path, but also at the interior positions where the path reaches a support that constraints the vertical displacement. SUPG is the only method that enables insertion of such constraints in the resulting system of algebraic equations (Eq. (23)). This property renders SUPG the only method that can be applied directly to such general finite element systems since it is the only capable of gathering the probability at the certain event of zero displacement at the supports. The results of this calculation are presented in the contour plots of the variance of the vertical displacement depicted in Fig. 22a, b for MCS and SUPG, respectively. These results demonstrate a fair accuracy of the SUPG with respect to the 'exact' MCS solution.

6 Conclusions

An alternative methodology of applying the probability density evolution method in general stochastic FE systems is outlined. With the proposed methodology the probability density function at a given position of the structure can be estimated via the solution of a series of pure advection pde's and thus, the complete probabilistic information of the system under consideration can be accurately and efficiently captured. In an attempt to increase the accuracy of the most frequently used finite difference LW schemes, which are used in order to solve the pde's involved in the method, two alternative Galerkin-based techniques were investigated, namely, the DG-FEM and the Streamline Upwind/Petrov Galerkin method. The results were compared to the LW equipped with the TVD property, as well as with brute force Monte Carlo Simulation. Our investigations showed SUPG to be more efficient, having higher convergence rates than the other two methods, while being the only method that could capture accurately the evolution of pdf near the boundaries of the structure.

Acknowledgments This work has been supported by the European Research Council Advanced Grant "MASTER-Mastering the computational challenges in numerical modeling and optimum design of CNT reinforced composites" (ERC-2011-ADG_20110209).

References

1. Au SK, Beck JL (2001) Estimation of small failure probabilities in high dimensions by subset simulation. Probab Eng Mech 16(4):263–277
2. Brooks AN, Hughes TJ (1982) Streamline upwind/Petrov–Galerkin formulations for convection dominated flows with particular emphasis on the incompressible Navier–Stokes equations. Comput Methods Appl Mech Eng 32(1–3):199–259
3. Chen JB, Li J (2008) Strategy for selecting representative points via tangent spheres in the probability density evolution method. Int J Numer Methods Eng 74(13):1988–2014

4. Chen JB, Li J (2009) A note on the principle of preservation of probability and probability density evolution equation. Probab Eng Mech 24(1):51–59
5. Chen JB, Zhang S (2013) Improving point selection in cubature by a new discrepancy. SIAM J Sci Comput 35(5):A2121–A2149
6. Chen JB, Ghanem R, Li J (2009) Partition of the probability-assigned space in probability density evolution analysis of nonlinear stochastic structures. Probab Eng Mech 24(1):27–42
7. Cho H, Venturi D, Karniadakis G (2013) Adaptive discontinuous galerkin method for response-excitation pdf equations. SIAM J Sci Comput 35(4):B890–B911
8. Cockburn B, Shu CW (1998) The local discontinuous Galerkin method for time-dependent convection-diffusion systems. SIAM J Numer Anal 35(6):2440–2463
9. Cockburn B, Shu CW (2001) Runge–Kutta discontinuous Galerkin methods for convection-dominated problems. J Sci Comput 16(3):173–261
10. Cockburn B, Lin SY, Shu CW (1989) TVB Runge–Kutta local projection discontinuous Galerkin finite element method for conservation laws III: one-dimensional systems. J Comput Phys 84(1):90–113
11. Courant R, Friedrichs K, Lewy H (1928) Über die partiellen differenzengleichungen der mathematischen physik. Math Ann 100(1):32–74
12. de Vahl Davis G, Mallinson G (1976) An evaluation of upwind and central difference approximations by a study of recirculating flow. Comput Fluids 4(1):29–43
13. Elman HC, Silvester DJ (2005) Finite elements and fast iterative solvers: with applications in incompressible fluid dynamics. Oxford University Press, Oxford
14. Ghanem R, Spanos P (1990) Polynomial chaos in stochastic finite elements. J Appl Mech Trans ASME 57(1):197–202
15. Hesthaven JS, Warburton T (2007) Nodal discontinuous Galerkin methods: algorithms, analysis, and applications, 1st edn. Springer Publishing Company, Incorporated
16. Houston P, Schwab C, Süli E (2000) Stabilized hp-finite element methods for first-order hyperbolic problems. SIAM J Numer Anal 37(5):1618–1643
17. Hughes TJ, Mallet M, Akira M (1986) A new finite element formulation for computational fluid dynamics: II. Beyond SUPG. Comput Methods Appl Mech Eng 54(3):341–355
18. Kleiber M, Hien TD (1992) The stochastic finite element method (basic perturbation technique and computer implementation). Wiley, Chichester
19. Kougioumtzoglou I, Spanos P (2012) An analytical Wiener path integral technique for non-stationary response determination of nonlinear oscillators. Probab Eng Mech 28:125–131
20. Kougioumtzoglou I, Spanos P (2014) Nonstationary stochastic response determination of nonlinear systems: a Wiener path integral formalism. J Eng Mech 140(9):04014064
21. Koutsourelakis P, Pradlwarter H, Schuëller G (2004) Reliability of structures in high dimensions, part I: algorithms and applications. Probab Eng Mech 19(4):409–417
22. LeVeque RJ (1992) Numerical methods for conservation laws, 2nd edn. Birkhäuser, Boston
23. LeVeque RJ (2002) Finite volume methods for hyperbolic problems. Cambridge texts in applied mathematics. Cambridge University Press, Cambridge
24. Li J, Chen JB (2004) Probability density evolution method for dynamic response analysis of structures with uncertain parameters. Comput Mech 34(5):400–409
25. Li J, Chen JB (2007) The number theoretical method in response analysis of nonlinear stochastic structures. Comput Mech 39(6):693–708
26. Li J, Chen JB (2008) The principle of preservation of probability and the generalized density evolution equation. Struct Saf 30(1):65–77
27. Papadopoulos V, Iglesis P (2007) The effect of non-uniformity of axial loading on the buckling behaviour of shells with random imperfections. Int J Solids Struct 44(18–19):6299–6317
28. Papadrakakis M, Kotsopoulos A (1999) Parallel solutions methods for stochastic fea using Monte Carlo simulation. Comput Methods Appl Mech Eng 168:305–320
29. Papadrakakis M, Papadopoulos V (1996) Robust and efficient solution techniques for the stochastic finite element analysis of space frames. Comput Methods Appl Mech Eng 134:627–658
30. Qiu J, Khoo BC, Shu CW (2006) A numerical study for the performance of the Runge–Kutta discontinuous Galerkin method based on different numerical fluxes. J Comput Phys 212(2):540–565
31. Raithby G (1976) A critical evaluation of upstream differencing applied to problems involving fluid flow. Comput Methods Appl Mech Eng 9(1):75–103
32. Reed W, Hill T (1973) Triangular mesh methods for the neutron transport equation. Tech Report. LA-UR-73-479, Los Alamos Scientific Laboratory
33. Roache PJ (1972) On artificial viscosity. J Comput Phys 10(2):169–184
34. Schenk C, Schuëller G (2003) Buckling analysis of cylindrical shells with random geometric imperfections. Int J Non-Linear Mech 38(7):1119–1132
35. Schneider-Bürger M (2003) Stahlbau-Profile. Stahleisen-Verlag, Dusseldorf
36. Schuëller G (2006) Developments in stochastic structural mechanics. Arch Appl Mech 75(10–12):755–773
37. Shinozuka M, Jan CM (1972) Digital simulation of random processes and its applications. J Sound Vib 25(1):111–128
38. Stavroulakis G, Giovanis DG, Papadrakakis M, Papadopoulos V (2014) A new perspective on the solution of uncertainty quantification and reliability analysis of large-scale problems. Comput Methods Appl Mech Eng 276:627–658
39. Venturi D, Karniadakis G (2012) New evolution equations for the joint response-excitation probability density function of stochastic solutions to first-order nonlinear pdes. J Comput Phys 231(21):7450–7474
40. Venturi D, Tartakovsky D, Tartakovsky A, Karniadakis G (2013) Exact pdf equations and closure approximations for advective-reactive transport. J Comput Phys 243:323–343
41. Wang P, Tartakovsky DM (2012) Uncertainty quantification in kinematic-wave models. J Comput Phys 231(23):7868–7880
42. Xu J, Chen JB, Li J (2012) Probability density evolution analysis of engineering structures via cubature points. Comput Mech 50(1):135–156